PIER B

Analysis of a Quad Port Dual Band MIMO Antenna for Sub-6 GHz Applications

Madhavareddy V. Narayana[1], Govardhani Immadi[1, *], Ambati Navya[1], Maringanti V. Swathi[2],
Muralidharan Nikhitha[1], Bhavanam Vineetha[1], and Gottapu C. A. S. Swaroop[1]

[1]*Department of ECE, KLEF, Vaddeswaram, Guntur, Andhra Pradesh, India*
[2]*Deptartment of ECE, NIT Silchar, Silchar, Assam, India*

ABSTRACT: A dual-band serrated microstrip MIMO antenna is proposed for 5th generation wireless applications in this article. Here, the designed MIMO antenna is a serrated basic microstrip patch antenna. The dual-band microstrip MIMO antenna is excited by utilising a $50\,\Omega$ transmission line. A full ground copper layer has been utilized in the design to attain a better isolation, whereas the fabricated antenna's isolation among the antenna elements is measured to be greater than $-20\,$dB. The simulated $-10\,$dB impedance bandwidth of $160\,$MHz (3.340–$3.50\,$GHz) and $220\,$MHz (5.50–$5.72\,$GHz) can cover 3.40–$3.60\,$GHz and 5–$5.7\,$GHz fifth generation bands. In addition, the measured ECCs are less than 0.0025 and 0.001 at the two resonant frequency bands and for the two MIMO antennas. The antenna diversity parameters covering ECC and DG were analyzed. The average gain for the single-element, dual-port and quad-port MIMO antennas is $3\,$dBi. These parameters make the serrated microstrip MIMO antenna also suitable for intelligent IOT devices operating in sub-6 GHz band.

1. INTRODUCTION

5G wireless communication systems have recently been extensively used and employed in various applications as a result of rapidly expanding wireless communication technology. With greater data speeds and reduced latency than 4G systems, 5G promises to offer seamless connection [1]. The two resonant frequency bands that were utilized in this application are the fifth generation and mm-wave frequencies. Because of its larger wavelength, higher penetration, and longer range midfrequency bands were extensively explored for the fifth generation communication technology. In Figure 1, the specifications of 5G are mentioned. 5G has been classified into 3 types based on the bandwidths which are represented in Table 1. Antenna design has a considerable challenge to obtain a small size with high data rate handling capabilities due to the constantly growing data capacity needs and the trend towards miniaturization of wireless communication systems. Adopting multiple-input multiple-output (MIMO) antennas, which improves both spectrum utilization and data speeds, is a practical solution to this issue [2–4]. Techniques to reduce mutual coupling and enhance isolation in a MIMO antenna among the antenna elements are necessary for the effective design of a spatial diversity in a MIMO antenna. The improvement of MIMO antenna isolation has been the subject of several studies. Several MIMO antennas obtain good isolation by maintaining the gap among the antenna elements at an appropriate level. In [5], improving isolation involved placing the antenna elements in mirror images and inserting a chip inductor among closely placed antennas. In

addition, grounding branches might change isolation and produce new coupling [6, 7]. When grounded branches are used, isolation in the low-frequency region may be improved, and the antenna's impedance can be better matched [6]. Additionally, a neutral line is frequently used to reduce mutual coupling coefficient [8–10]. By connecting a close-by orthogonal pair of antenna components with some basic neutral line, high isolation may be achieved [10]. Defected Ground Structure (DGS) can further enhance isolation by altering γ_r of the substrate; this method is widely used to prevent undesired coupling [11–14]. Multi-slotted decoupling antenna design [15], generic decoupling design [16], rectangular microstrip stub [17], and other special decoupling structures are used by some MIMO antennas to enhance isolation. The antenna reported in a research paper [18] included grounded, quarter-wavelength strip resonators, increasing isolation between the antenna parts at the expense of bandwidth. Although they are too complicated to be employed in miniaturized antennas, meta-surfaces and Electromagnetic Band-Gap (EBG) type antennas are nevertheless useful techniques for enhancing isolation [19, 20]. In conclusion, a major issue still exists in the medium-size MIMO antenna system design process to achieve acceptable isolation. Figure 2 presents the classification of the antenna based on input-output port.

The design and analysis of single element, dual-port and quad-port serrated microstrip MIMO antennas are examined in this work. The optimization of a single element antenna design is followed by the replication of that antenna geometry in both the horizontal and vertical directions to design two and four element MIMO antennas. S-parameters and other MIMO antenna parameters were measured in terms of Envelope Cor-

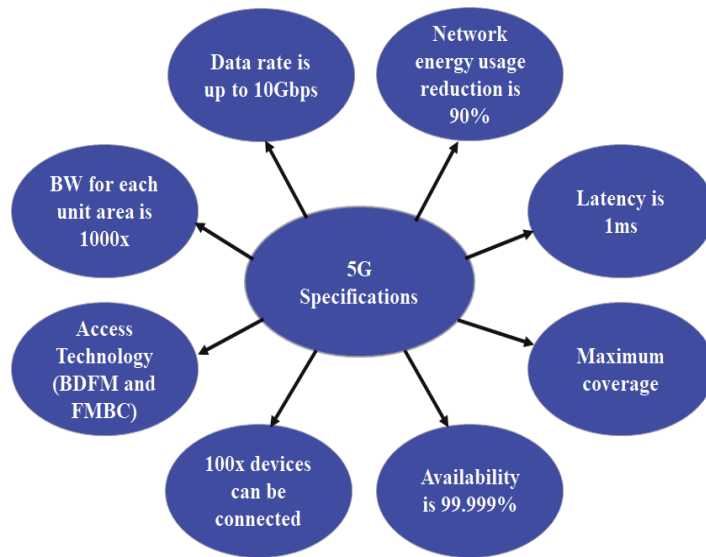* Corresponding author: Govardhani Immadi (govardhanee_ec@kluniversity .in).
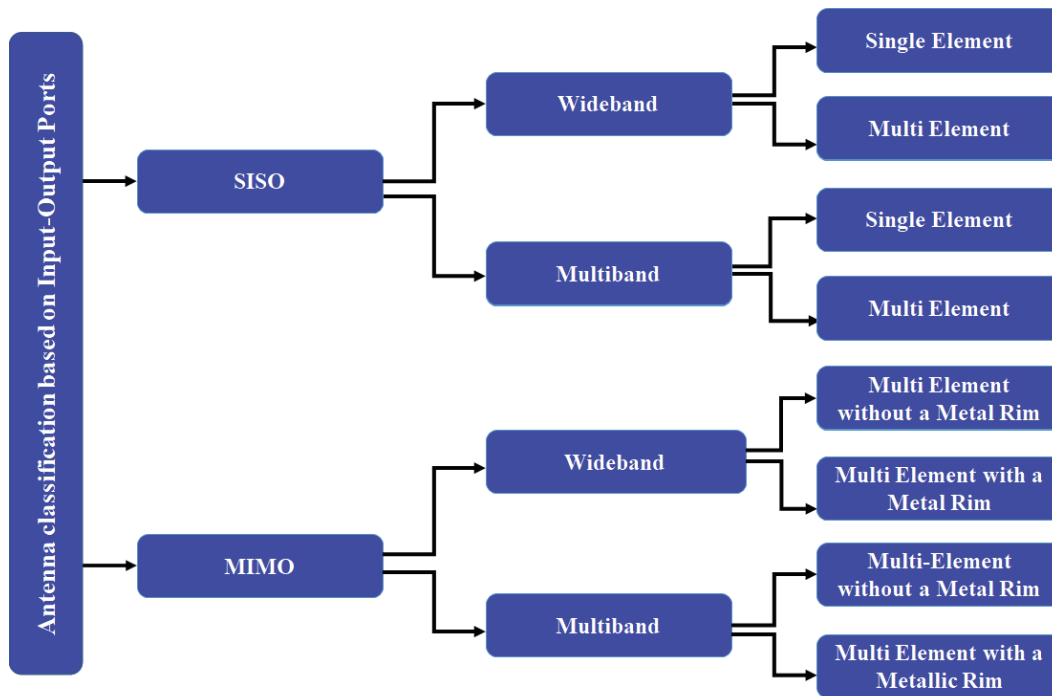
FIGURE 1. Specifications of 5G.

FIGURE 2. Classification of the antenna based on input-output port.

TABLE 1. 5G frequency bands.

S No.	Name	Frequency range
1	Low band	< 1 GHz
2	Mid band	1–6 GHz
3	High band	24–40 GHz

relation Coefficient (ECC) and Diversity Gain (DG), and all of the results are consistent with the values shown in [20–22]. A substrate integrated frequency selective surface antenna has been designed for Internet of Things (IOT) applications using CST Microwave studio [23]. A low-profile dual-band electrically small antenna has been designed for Radio Frequency Identification (RFID) applications [24]. A low-profile electrically small antenna with a circular slot for global positioning system applications [25] has been designed with $ka < 1$. A compact multiband hybrid rectangular Dielectric Resonator Antenna (DRA) for wireless applications, different dielectric resonator antennas has been designed for various wireless communication applications [26]. A compact electrically small antenna with split ring resonators has been designed for RFID applications [27]. An electrically small serrated rectangular patch antenna has been designed for RFID applications [28].
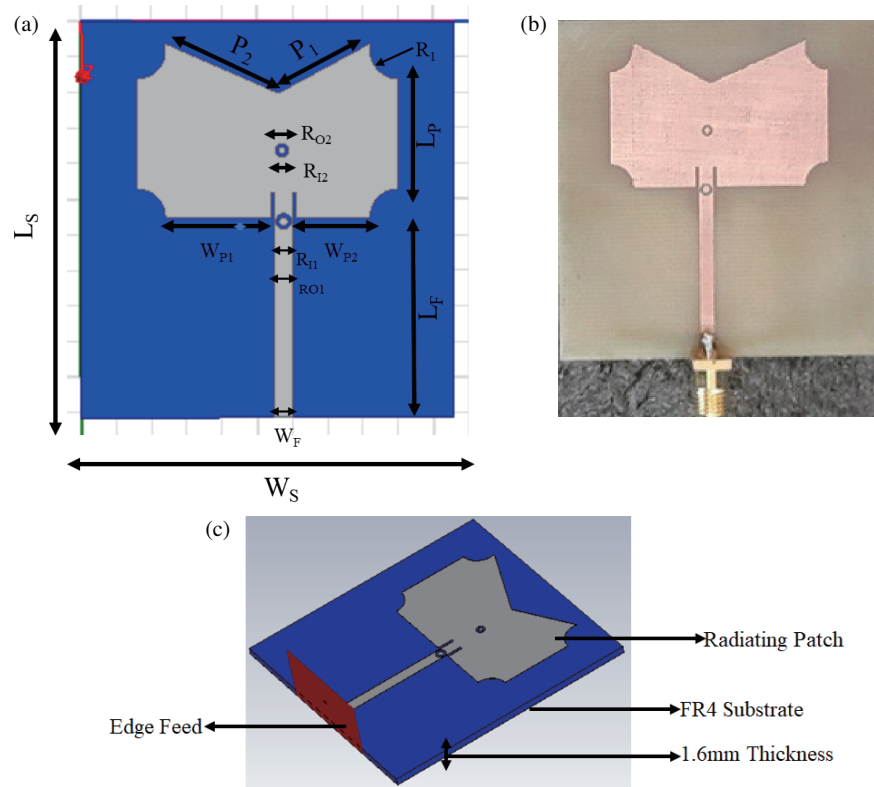
FIGURE 3. Single-element serrated microstrip antenna. (a) Designed antenna. (b) Faricated antenna. (c) Tilted view.

TABLE 2. Measurements of the single-element serrated microstrip antenna.

S. No	Variables	Values (mm)
1	Length of the conducting plane (L_S)	55.56
2	Width of the conducting plane (W_S)	52.92
3	Length of the radiating element (L_P)	24.42
4	Length of feedline (L_F)	31.56
5	Width of patch (W_P)	37
6	Width of patch 2 (W_{P2})	10.5
7	Width of feedline (W_F)	2.47
8	Radius of outer circle 1 (R_{O1})	1.1
9	Radius of inner circle 1 (R_{I1})	0.6
10	Radius of outer circle 2 (R_{O2})	0.95
11	Radius of inner circle 2 (R_{I2})	0.5
12	Radius of circle on the sides of the patch (R_1)	4

The following is the order of this article. In Section 2, a single element antenna and how it evolves from a fundamental microstrip patch antenna are shown. Section 3 presents the performance of the fundamental antenna configurations as well as additional MIMO diversity features. Thereby the paper is concluded in Section 4.

2. ANTENNA DESIGN TOPOLOGY

This section discussed the design processes of the serrated microstrip MIMO antenna, the substrate used, and the antenna's material properties.

Figure 3 shows a single-element microstrip antenna from the top and tilted view. This antenna contains a serrated basic microstrip patch antenna united by a microstrip transmission line having an impedance of $50\,\Omega$. FR4 epoxy material with a thickness of 1.6 mm was used as the substrate owing to its material properties, such as γ_r of 4.4 and loss tangent ($\tan\delta$) of 0.02. Full ground has been used for designing the serrated microstrip antenna. The dimensions utilized in designing the serrated microstrip antenna are shown in Table 2.

Figure 4 shows the serrated microstrip patch antenna's step-by-step design. In step 1, a basic microstrip patch united to the feedline is realized. Step 1 antenna works at 2.80 GHz
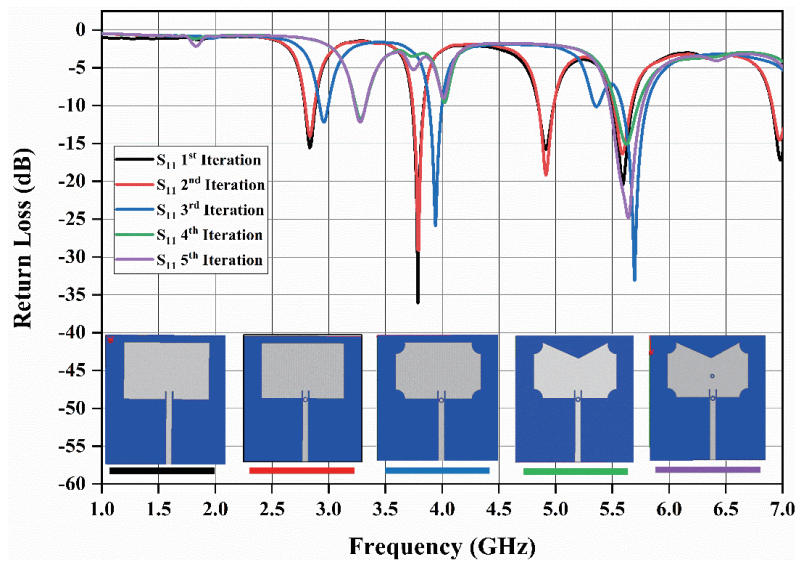
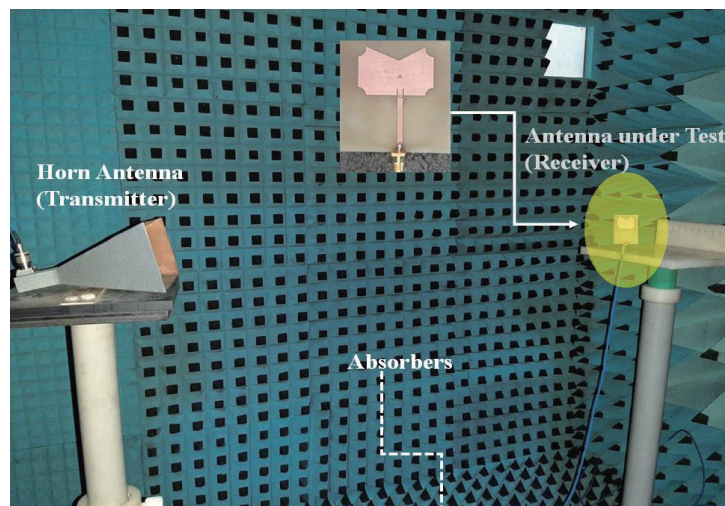**FIGURE 4**. Evolution of the serrated microstrip antenna.

FIGURE 5. Radiation pattern measurement of single-element serrated microstrip MIMO antenna utilising anechoic chamber.

with S_{11} of -15.45 dB, at 3.7 GHz with S_{11} of -35.45 dB, at 4.8 GHz with S_{11} of -15.02 dB, at 5.596 GHz with S_{11} of -20.44 dB, and at 6.9 GHz with S_{11} of -16.92 dB. In step 2, the step 1 design is modified by adding a circular structure on the feedline to the existing design. The radius of the outer circle (represented by RO1) is 1.1 mm, and the radius of the inner circle is 0.6 mm. The step 2 antenna operates at 2.80, 3.70, 4.90, 5.50, and 6.90 GHz with S_{11} of -13.76 dB, -28.5 dB, -18.6 dB, -16.1 dB, and -14.2 dB. In the third iteration, four arcs are removed from the four sides of the patch with a radius of 4 mm. Step 3 antenna functions at 2.950 GHz with S_{11} of -12.17 dB, at 3.9 GHz with S_{11} of -25.1 dB, at 5.6 GHz with S_{11} of -33.03 dB, and at 7.23 GHz with S_{11} of -32.2 dB. In the fourth iteration, a triangular structure has been removed from the patch. The antenna operates at 5.60 GHz with S_{11} of -15.1 dB and at 3.3 GHz with S_{11} of -11.57 dB in the fourth iteration. The frequency obtained above 6 GHz have been elim-

inated achieving the goal of this work. In the fifth iteration, a concentric circle is added to the patch in the center with a radius of 0.95 mm, and 0.5 mm radian circle is subtracted from the inner circle. This step was done to improvise the S_{11} at the same frequency. At 3.30 GHz, the S_{11} of -11.57 dB has changed to -12 dB in the final iteration, while at 5.60 GHz, the S_{11} of -15.1 dB has changed to -24.54 dB. The serrated microstrip antenna design fulfilling all the requirements is considered as the final proposed design. Figure 4 provides the consolidated result of the return loss at each step in a single graph for clear understanding of the serrated microstrip antenna.

To design a dual-port serrated microstrip MIMO antenna, the single element serrated microstrip MIMO antenna is replicated along the horizontal axis. There are multiple elements in the MIMO antenna, which will provide multiple data streams to transmit and receive large amount data simultaneously. To achieve the spatial diversity seen in Figure 6, the inter-element
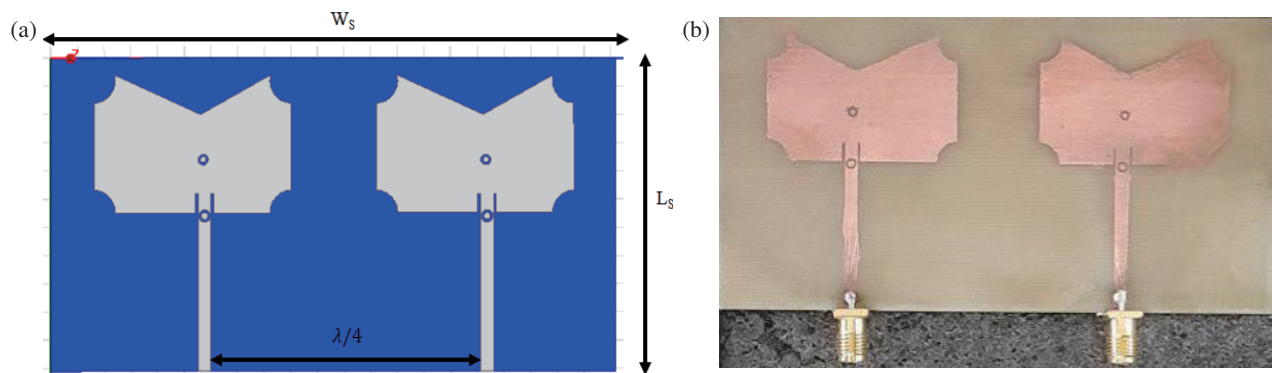
FIGURE 6. Dual-element serrated microstrip MIMO antenna. (a) Simulated. (b) Manufactured design.
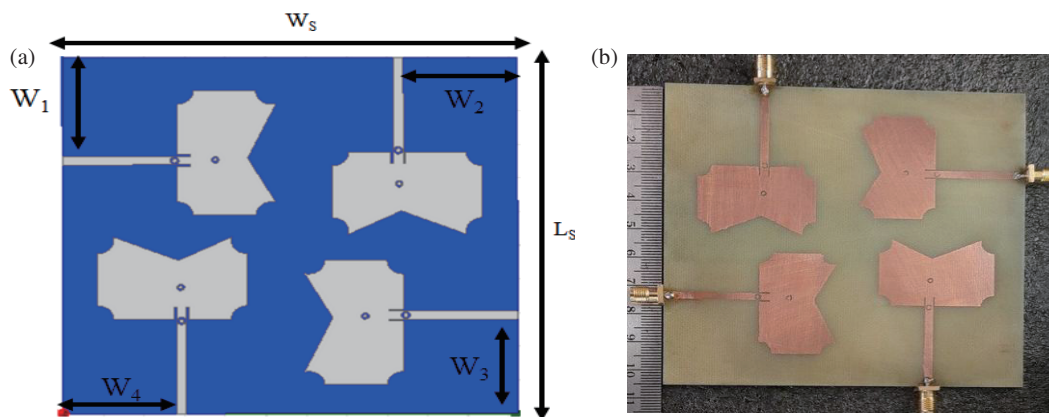

FIGURE 7. Quad-element serrated microstrip MIMO antenna. (a) Simulated. (b) Manufactured design.

distance between two elements was kept at $\lambda/4$. The antenna's design is made more challenging because it was found that no further isolation techniques were needed. This dual-port antenna has a size of $55.56 \times 105.84 \times 1.6 \, \text{mm}^3$. The simulated and fabricated dual-port serrated microstrip MIMO antennas are shown in Figure 6. The antenna is further modified by replicating two elements along the vertical-axis to obtain a four-element serrated microstrip MIMO antenna. The inter element spacing of $\lambda/4$ has been maintained along x-axis and y-axis antenna elements. These four elemental MIMO antennas have a size of $111.12 \times 105.84 \times 1.6 \, \text{mm}^3$. Figure 7 represents the simulated and fabricated designs of the two-element serrated microstrip MIMO antenna.

3. RESULTS & DISCUSSIONS

This part is separated into subsections that give a detailed explanation of the simulated results and the conclusions that can be made from the simulated outcomes.

3.1. Single-Element Serrated Microstrip Antenna

The final iteration antenna is manufactured on FR4 epoxy material as represented in Figure 5. Ground layer is a plain copper layer, and the top layer is a serrated microstrip antenna. These two are attached by utilizing an SMA connector.

The whole purpose of manufacturing the prototype of the design was to compare the simulated and fabricated results of the antenna parameters and other diversity parameters. While comparing the simulated and fabricated MIMO antennas in Figure 8, the simulated antenna operates at 3.30 GHz with S_{11} of $-12 \, \text{dB}$ and at 5.60 GHz with S_{11} of $-24.54 \, \text{dB}$ whereas the prototype works at 3.280 GHz with S_{11} of $-11.72 \, \text{dB}$ and at 5.60 GHz with $-20.9 \, \text{dB}$. There is a slight difference in the results, which is caused by the equipment and manufacturing deviations at calibration level. Overall, the simulated and fabricated results are in close agreement between each other. The proposed serrated microstrip antenna is suitable in various other countries like Japan, Russia, and China for IOT devices working under sub-6 GHz 5G band.

Voltage Standing Wave Ratio (VSWR) is one of the vital parameters of an antenna. Figure 9 presents the simulated and measured VSWRs of the unit-element serrated microstrip antenna. The typical value of VSWR must be in the range of 0–2. The simulated and fabricated VSWRs for the single element antenna at 3.30 GHz are 1.67 and 1.68, respectively, and for 5.6 GHz are 1.14 and 1.3, respectively. The radiation pattern of the serrated microstrip antenna is measured by placing it in an anechoic chamber. Figure 10 illustrates the radiation pattern of implemented design in E-plane and H-plane at 3.30 GHz and 5.60 GHz. In both the principal plane (E&H), there is good co-pol and cross-pol difference in broadside direction, i.e., more
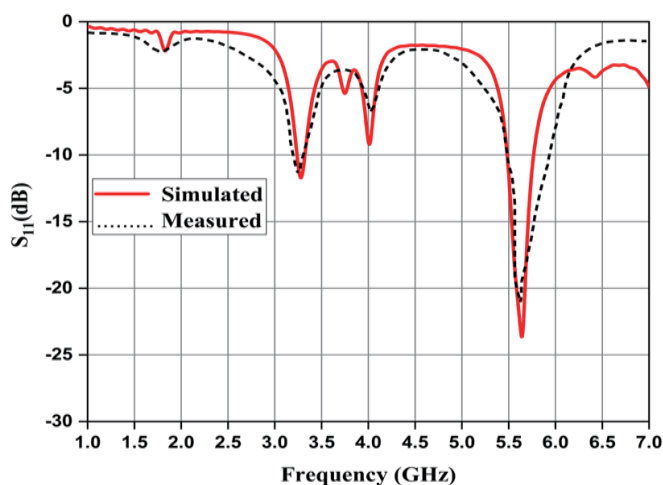
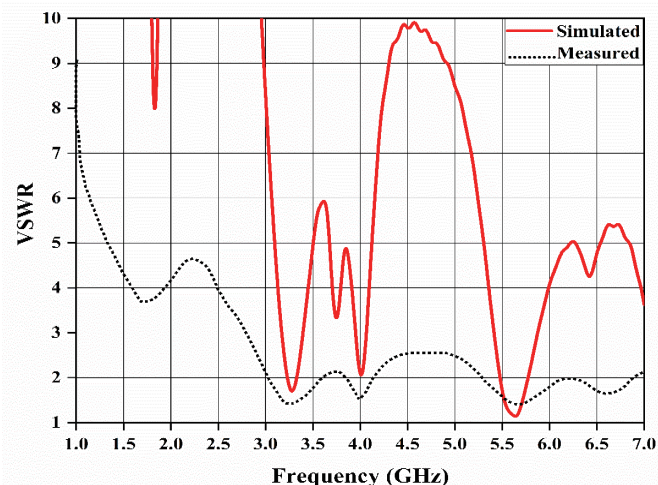**FIGURE 8**. Simulated and fabricated S_{11} of the single-element serrated microstrip antenna.

FIGURE 9. Simulated and fabricated VSWR of the single-element serrated microstrip Antenna.
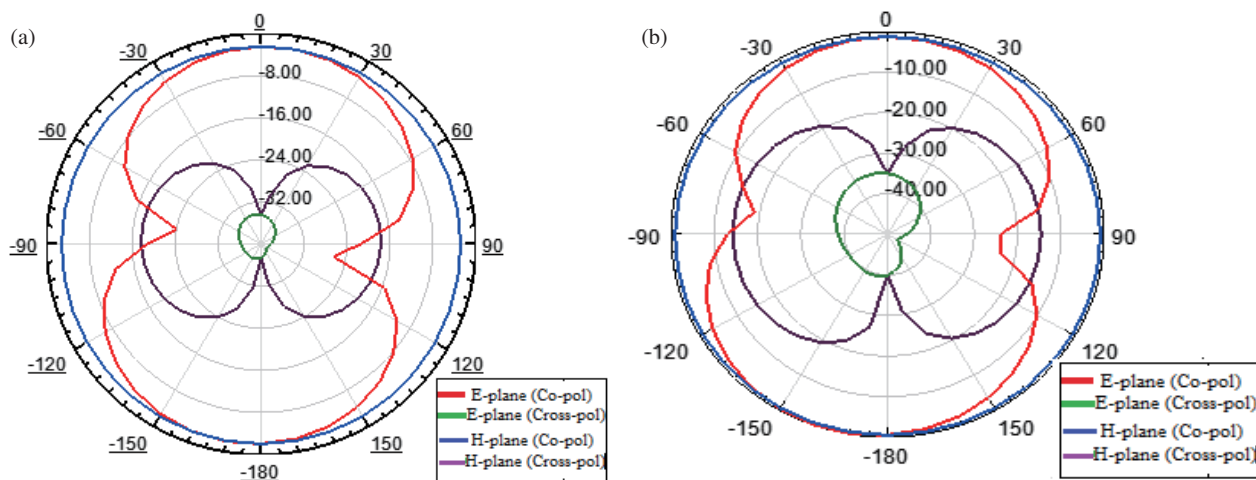

FIGURE 10. Simulated and Measured radiation pattern of the single-element serrated microstrip antenna. (a) at 3.3 GHz, (b) at 5.6 GHz.

than 20 dB at all three frequency bands. It can be seen from Figure 10 that the radiations in E- and H-planes are omnidirectional at the two resonant frequency bands. The presented model has good radiation properties. The J-surface distribution is shown in Figure 11 at 3.3 and 5.6 GHz, respectively. The J-surf distribution is symmetrical throughout the patch and the feedline in a λ resonant mode concluding the antenna to be efficient. Figure 12 presents the 3-dimensional gain of the antenna at 3.3 and 5.6 GHz, respectively.

3.2. Dual-Port Serrated Microstrip Antenna

The fabricated prototype of the dual-port serrated microstrip MIMO antenna is presented in Figure 6. This section examines the performance of a dual-port serrated microstrip MIMO antenna in terms of S_{11}, S_{21}, VSWR, radiation pattern, gain, and surface current distributions, as well as other MIMO antenna parameters like ECC and DG. Figure 13 presents the simulated and fabricated S_{11} of the dual-port serrated microstrip MIMO antenna. The simulated antenna operates at 3.3 GHz with S_{11}

of -14.4 dB and at 5.6 GHz with S_{11} of -24.94 dB whereas the fabricated design functions at 3.28 GHz with S_{11} of -14 dB and at 5.62 GHz with -23.7 dB. Figure 14 represents the simulated and fabricated S-parameters of the serrated microstrip patch antenna.

Figure 15 presents the simulated and fabricated VSWRs of the two-element serrated microstrip MIMO antenna. The simulated and fabricated VSWRs at 3.30 GHz are 1.71 and 1.8, and at 5.6 GHz they are 1.17 and 1.21, respectively, which concludes the antenna having satisfactory results. Figure 16 presents the measurement of the reflection coefficient of a dual-port serrated microstrip MIMO antenna by using MS2037C Anritsu-Combinational Analyzer. Figure 17 presents the radiation pattern of a dual-port serrated microstrip MIMO antenna, and Figure 18 shows the surface current distribution of dual-port serrated microstrip MIMO antenna at each port for 3.30 and 5.60 GHz. Figure 17 illustrates the radiation pattern of implemented design in E-plane and H-plane at 3.30 GHz and 5.60 GHz. In both the principal planes ($E\&H$), there is
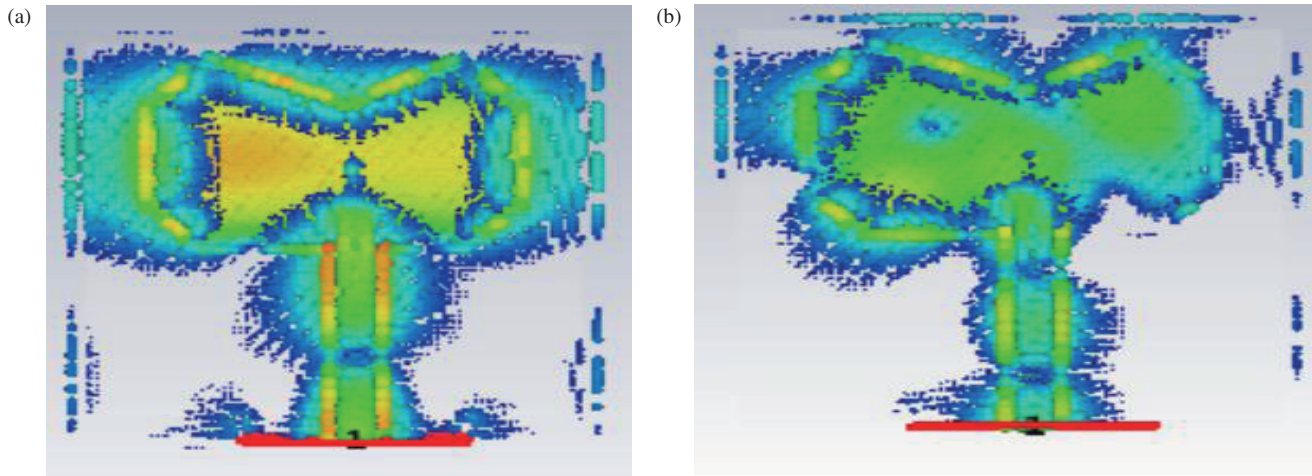
(a)

(b)

FIGURE 11. J-Surf Distribution of the single-element antenna. (a) 3.30 GHz, (b) 5.60 GHz.
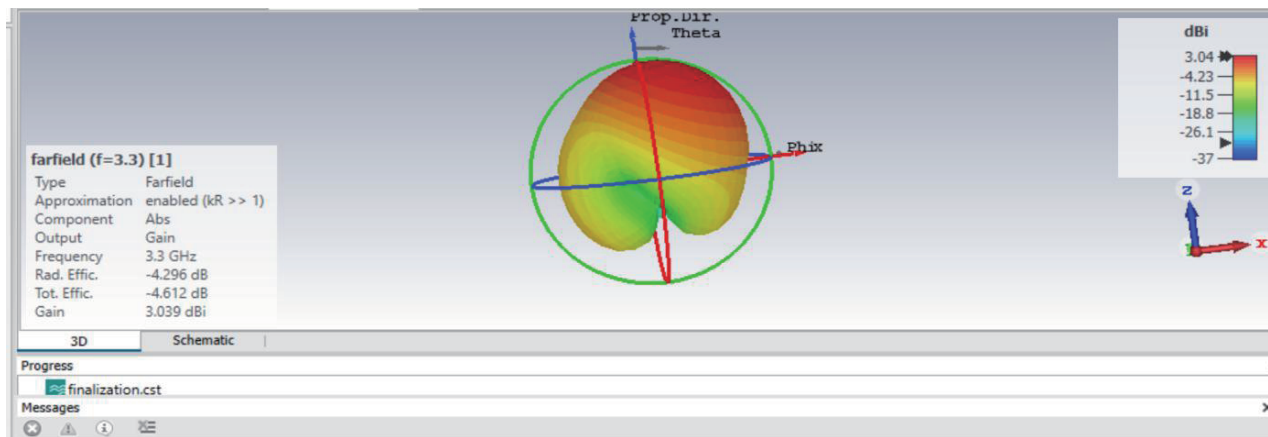

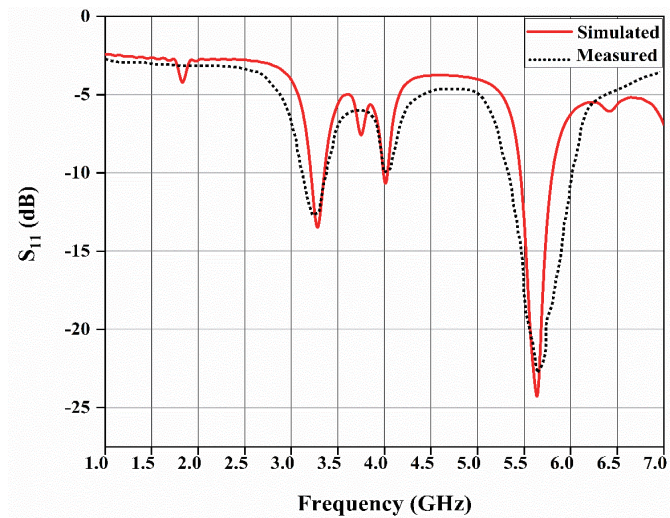**FIGURE 12**. 3-dimensional gain of the single-element serrated microstrip antenna.

FIGURE 13. Simulated and fabricated S_{11} of the dual-element serrated microstrip MIMO antenna.
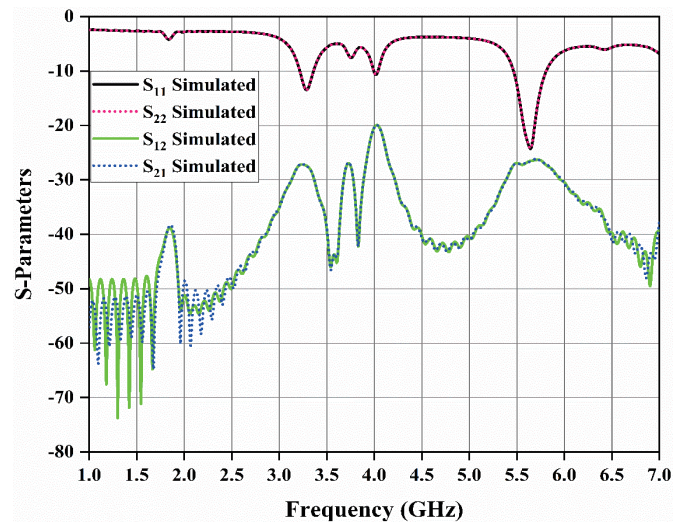

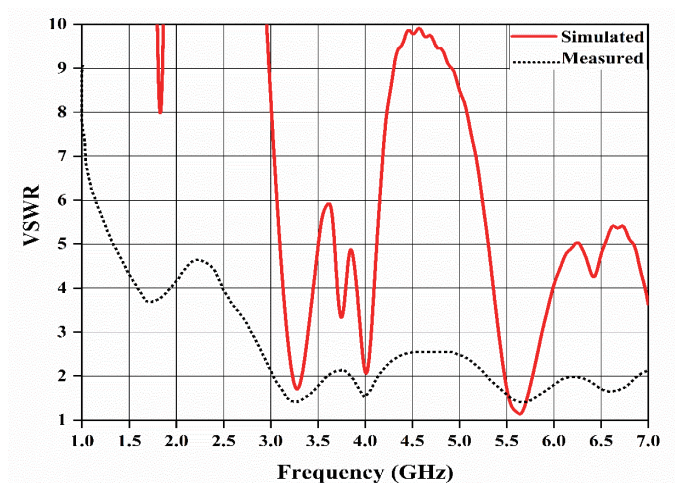**FIGURE 14**. S-parameters of the dual-element serrated microstrip MIMO antenna.

FIGURE 15. Simulated and fabricated VSWR of the dual-element serrated microstrip MIMO.
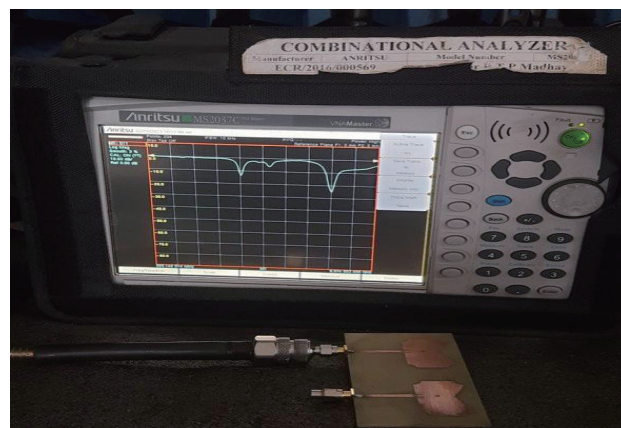

FIGURE 16. Measurement of S_{11} results by MS2037C anritsu combinational analyser.
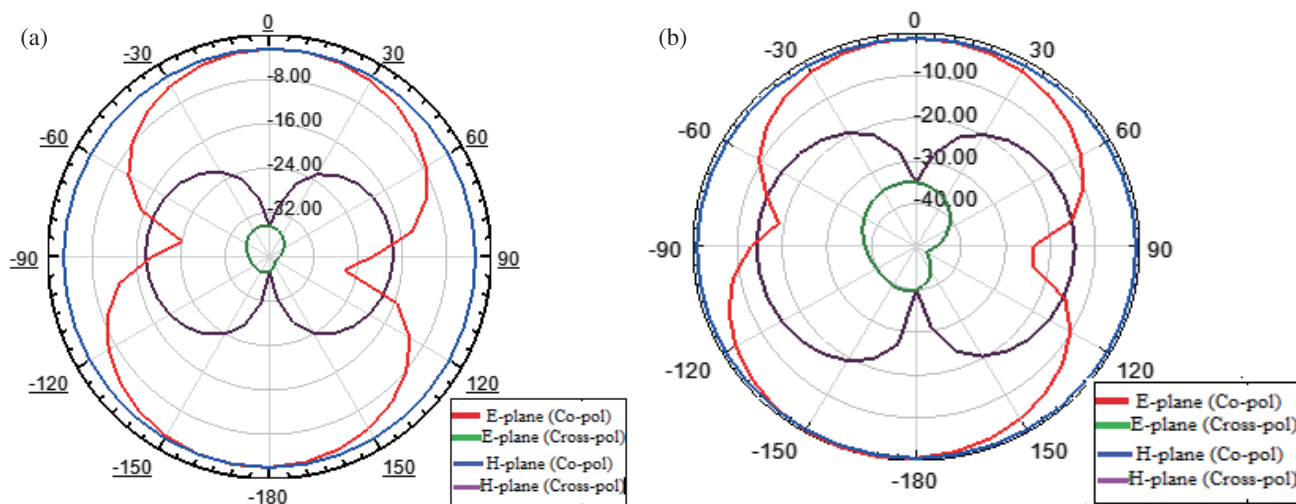

FIGURE 17. Simulated and measured radiation patterns of a dual-elemental serrated microstrip MIMO antenna. (a) at 3.3 GHz (b) at 5.6 GHz.

good co-pol and cross-pol difference in broadside direction, i.e., more than 20 dB at all three frequency bands. It can be seen from Figure 17 that the radiations in E- and H-planes are omni-directional at the two resonant frequency bands. The presented model has good radiation properties. Figure 18 shows the J-surface distribution of a dual-port serrated microstrip MIMO antenna. It has been demonstrated that there is essentially no coupling between the two antenna components when the primary port is fed, and the secondary port is terminated with a 50 Ω matching impedance. Lower mutual coupling is obtained by maintaining the distance between the antenna components. Figure 19 presents the 3-dimensional gain of the dual-port serrated microstrip MIMO antenna at 3.3 and 5.6 GHz, respectively.

3.3. Four-Element Serrated Microstrip Antenna

The fabricated prototype of the quad port serrated microstrip MIMO antenna is presented in Figure 7. The four-element

MIMO antenna performances by means of S_{11}, S_{21}, VSWR, radiation pattern, gain, and J-Surface distributions along with the other MIMO antenna parameters like ECC and DG are analyzed in this section. Figure 20 presents the simulated and fabricated S_{11} of the four-element serrated microstrip MIMO antenna. The simulated and prototype designs resonate at 3.3 GHz with S_{11} of -16.3 dB and -15 dB, respectively, and at 5.6 GHz frequency they resonate at -26.82 dB and -24.8 dB, respectively. From Figure 21, we observe that S_{11}, S_{22}, S_{33}, S_{44} at 3.3 GHz and 5.6 GHz are -16.3 dB and -26.82 dB, respectively. The isolation coefficient at 3.3 GHz ranges from -30 dB to -43 dB, and for 5.6 GHz it ranges from -33 dB to -53.5 dB. Figure 22 presents the measurement of the S_{11} of a quad-port serrated microstrip MIMO antenna by using MS2037C Anritsu-Combinational Analyzer. Figure 23 presents the simulated and fabricated VSWRs of the four-elemental serrated microstrip MIMO antenna. In Figure 23, the VSWRs of the simulated design at 3.3 GHz and 5.6 GHz are 1.62 and 1.15, respectively, and VSWRs of the prototype at 3.3 and 5.6 GHz
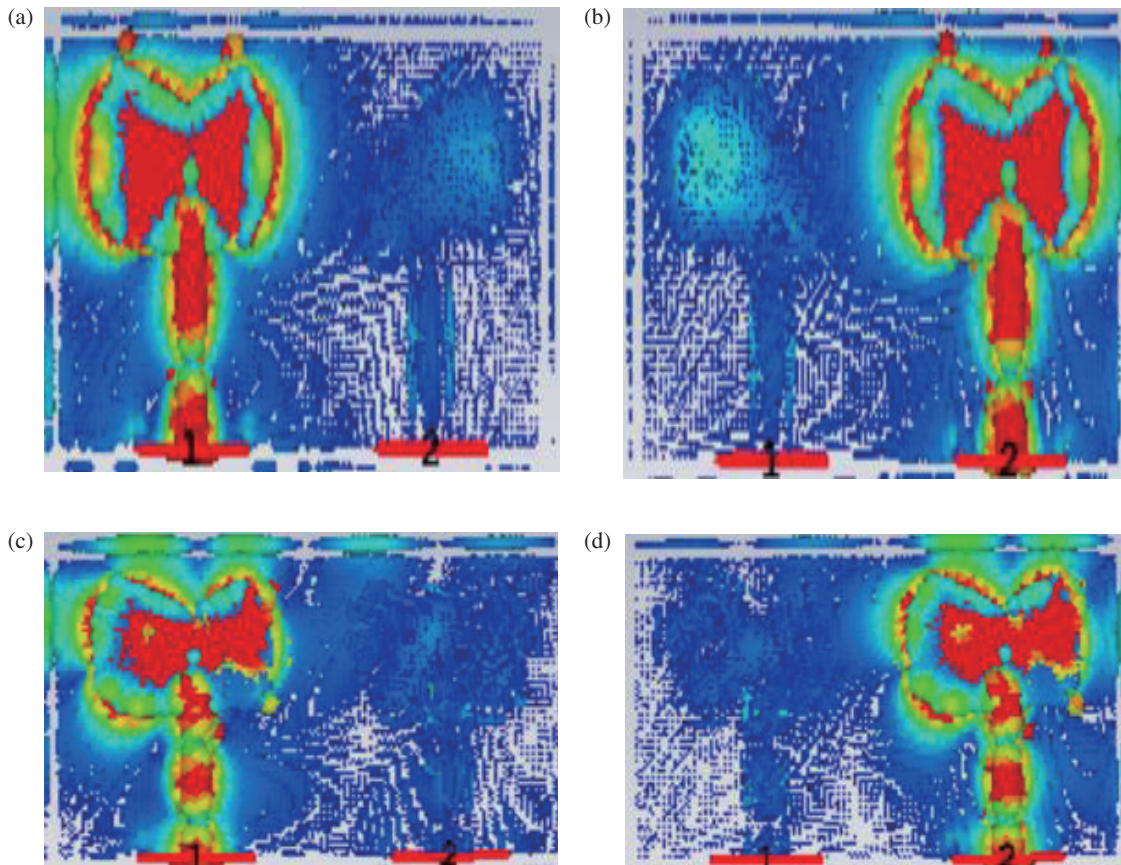
(a) (b)

(c) (d)

FIGURE 18. J-surface distribution of a dual-elemental serrated MIMO antenna (a), (b) 3.3 GHz, (c), (d) 5.6 GHz.
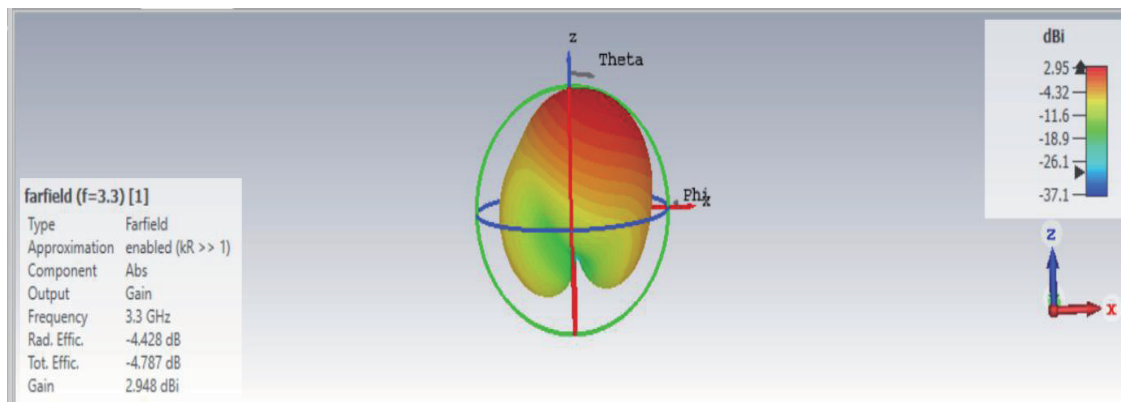
FIGURE 19. 3D gain of the dual-element serrated microstrip MIMO antenna.

are 1.58 and 1.19, respectively. The radiation patterns of simulated and fabricated antennas at 3.3 and 5.6 GHz are presented in Figure 24. Figure 24 illustrates the radiation pattern of implemented design in E-plane and H-plane at 3.30 GHz and 5.60 GHz. In both the principal planes ($E\&H$), there is good co-pol and cross-pol difference in broadside direction, i.e., more than 20 dB at all three frequency bands. It can be seen from Figure 24 that the radiations in E- and H-planes are omnidirectional at the two resonant frequency bands. The presented model has good radiation properties. Figure 25 presents

the distribution of surface current on the serrated microstrip MIMO antenna at each port. Figures 25(a)–(d) are for 3.3 GHz and (e)–(h) for 5.6 GHz. The J-surface distribution of a quad-port serrated microstrip MIMO antenna is presented in Figure 25. When the first port is fed by keeping the remaining three ports terminated with a 50 Ω matching impedance, it is noticed that the coupling among the four antenna components is minimal. Lower mutual coupling is attained by maintaining the distance between the antenna components. Figure 26
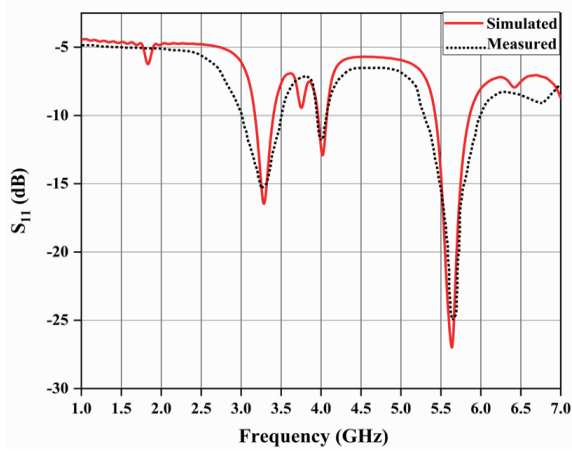
FIGURE 20. Simulated and fabricated S_{11} of the quad-element serrated microstrip patch antenna.
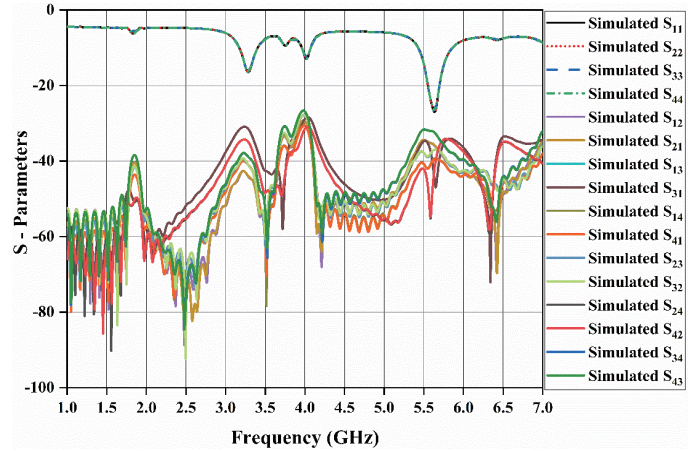
FIGURE 21. S-parameters of the quad-element serrated microstrip MIMO antenna.
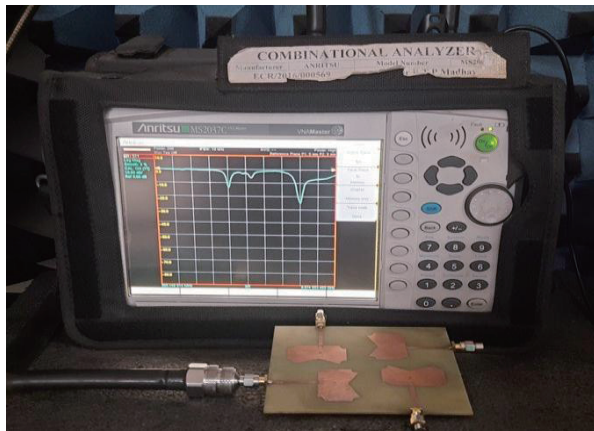
FIGURE 22. Measurement of S_{11} results by MS2037C anritsu combinational analyser.
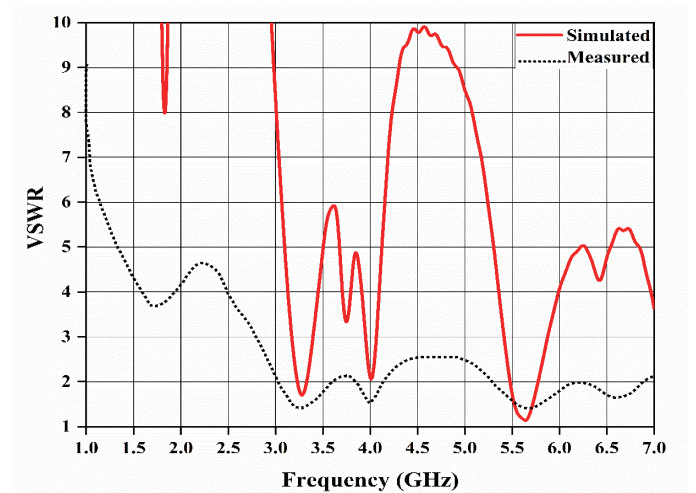
FIGURE 23. Simulated and fabricated VSWR of the four-port serrated microstrip MIMO antenna.

FIGURE 24. Simulated and measured radiation patterns of a four-elemental serrated microstrip MIMO antenna. (a) 3.3 GHz (b) 5.6 GHz.

FIGURE 25. Surface current distribution of a four-elemental serrated microstrip MIMO antenna. (a), (b), (c), (d) 3.3 GHz, (e), (f), (g), (h) 5.6 GHz.

FIGURE 26. 3D gain of the quad-element serrated microstrip MIMO antenna.

FIGURE 27. ECC and DG for dual-port MIMO antenna.

presents the 3-dimensional gain of the four-elemental serrated microstrip MIMO antenna at 3.3 and 5.6 GHz.

3.4. Analysis of MIMO Diversity Parameters

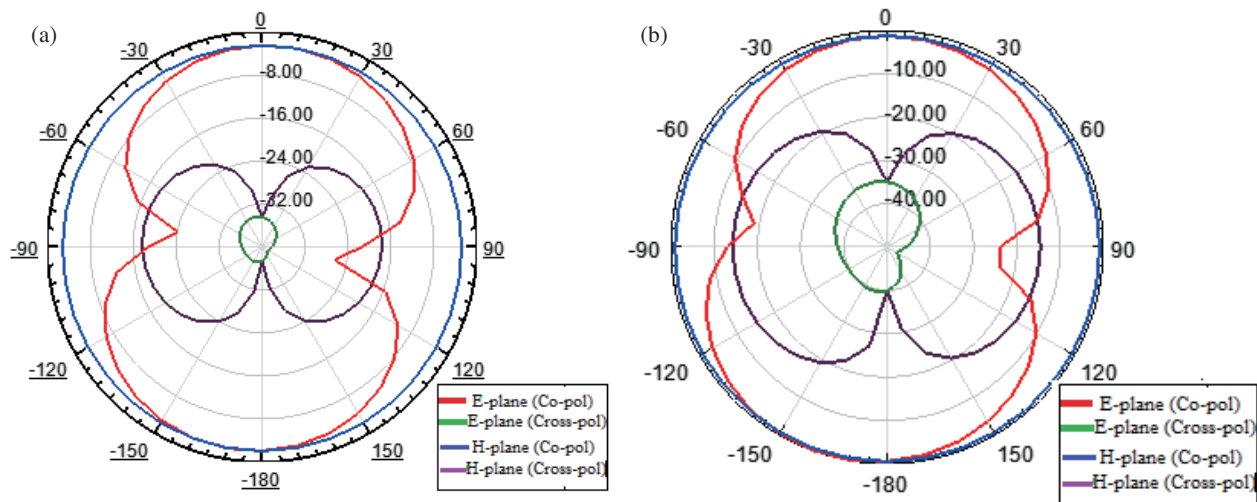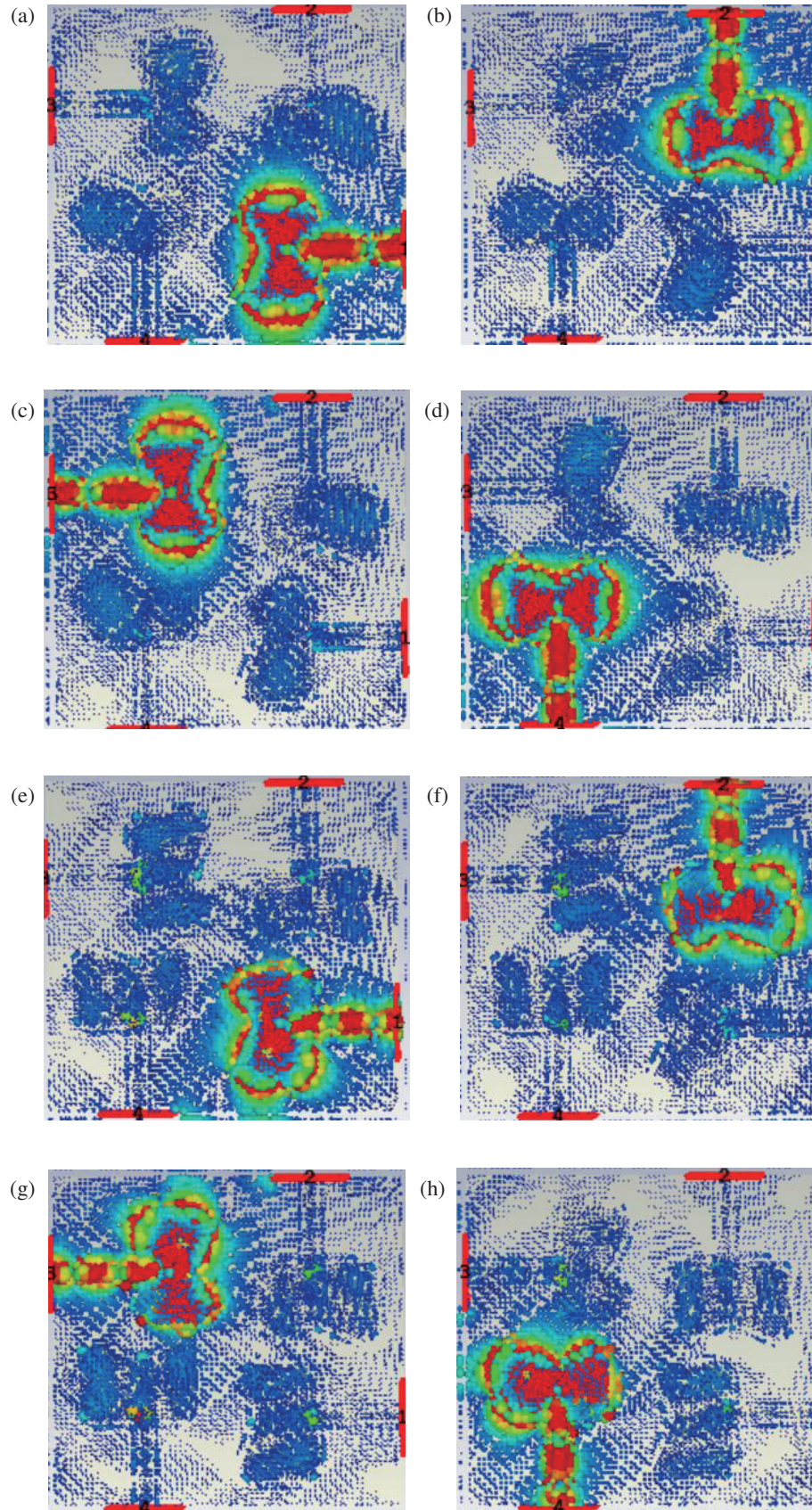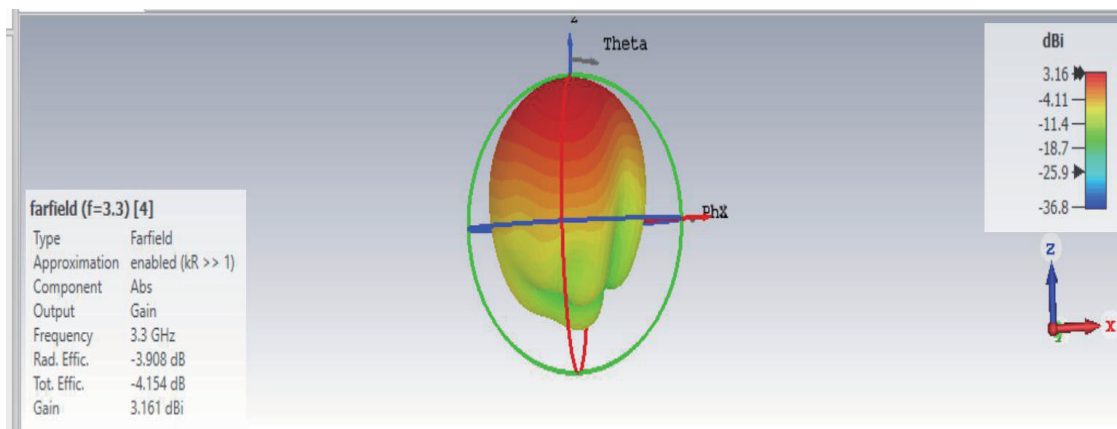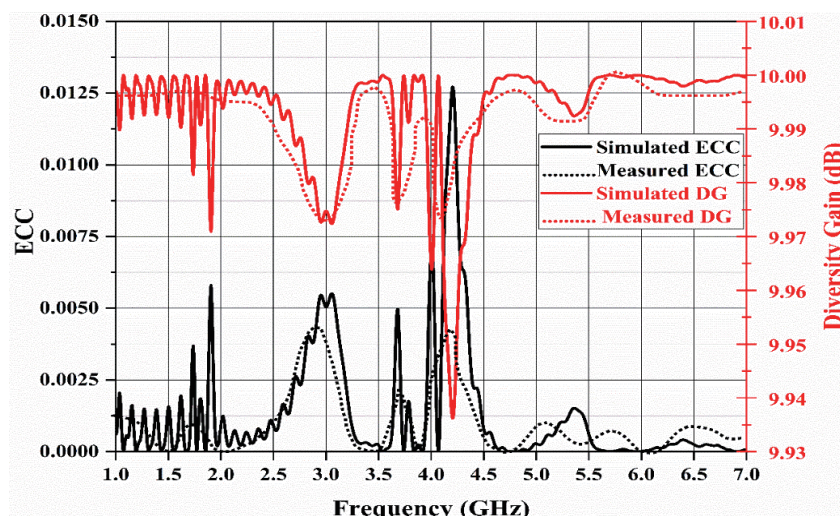When the effectiveness of MIMO diversity parameters is measured, ECC and DG are used to guarantee that the designed antenna satisfies the specifications outlined in [15–19].

ECC is a significant parameter to access the performance of a MIMO antenna. It determines the correlation with the neighbouring elements present in the design. The typical value of ECC is 0, but it can be ranged between the values of 0 to 0.5. It can be calculated in two ways either by using S-parameters or by using radiation pattern measurement. This is the formula for ECC according to the S-parameters

$$\rho_e = \frac{|S_{11}^* S_{12} + S_{21}^* S_{22}|^2}{(1 - |S_{11}|^2 - |S_{21}|^2)(1 - |S_{22}|^2 - |S_{12}|^2)}$$

$$ECC_{qp} = \frac{\left| \int\limits_0^{2\pi} \int\limits_0^{\pi} \left(E_{\theta p}^* E_{\theta q} P_\theta XPR + E_{\varphi p}^* E_{\varphi q} P_\varphi \right) d\Omega \right|^2}{\alpha \times \beta}$$

The above formula is for ECC as per the radiation pattern data.

$$\alpha = \int\limits_0^{2\pi} \int\limits_0^{\pi} \left(E_{\theta q}^* E_{\theta q} P_\theta XPR + E_{\varphi q}^* E_{\varphi q} P_\varphi \right) d\Omega$$

$$\beta = \int\limits_0^{2\pi} \int\limits_0^{\pi} \left(E_{\theta p}^* E_{\theta q} P_\theta XPR + E_{\varphi p}^* E_{\varphi q} P_\varphi \right) d\Omega$$

Diversity gain indicates the quality and reliability of a MIMO antenna. It is calculated by considering the values of ECC. Its ideal value should be 10 dB.

$$DG = 10 \times \sqrt{1 - |ECC_{qp}|^2}$$

Figure 27 presents the ECC and DG of the dual-port serrated microstrip MIMO antenna. The DG value of the two-port MIMO antenna is 9.93 which meets the MIMO diversity criteria. In addition, the ECCs of measured antennas are less than 0.0025 at both the resonant frequency bands.

148

TABLE 3. Comparison table of the proposed MIMO design to existing MIMO designs.

| References	Element	Bandwidth	Dimensions (mm²)	Return Loss	Gain (dBi)	ECC	DG (dB)
[14]	1	4.60–4.94 GHz	35 × 25	−19.53 dB	—	—	—
	2	Case 1: 4.65 to 4.97 GHz	Case 1: 50 × 35	Case 1: −17.44 dB	1.83	0.02	9.96
		Case 2: 4.67–4.94 GHz	Case 2: 70 × 25	Case 2: −17.44 dB	1.65	0.02	9.94
[15]	1	3.1–11.6 GHz	36 × 45	> 20 dB	—	—	—
	2	3.2–11.2 GHz	81 × 42	> 20 dB	5.2–9.20	< 0.15	—
	4	3.01–12.5 GHz	81 × 87	> 20 dB	5 to 9	< 0.2	—
[16]	4	3–4 GHz	160 × 160	< 20 dB	1.79–2.39	< 0.1	—
[17]	1	0.81–0.970 GHz	130 × 90	> 18 dB	—	—	—
		1.660–1.680 GHz		> 18 dB			
		2.670–3.530 GHz		> 18 dB			
		5.40–5.950 GHz		> 18 dB			
		6.73–6.88 GHz		> 18 dB			
	4	0.65–1 GHz	180 × 180	> 13 dB	−0.05	—	—
		2.5–3.5 GHz		> 13 dB	4.4		
		5–6.5 GHz		> 13 dB	6.9		
		6.5–7 GHz		> 13 dB	5.0		
[18]	4	3–5.5 GHz	180 × 80	< −30 dB	9.8–11.25	0.016	> 9.9
[19]	4	3.2–6 GHz	175 × 150	< −10 dB	2.5–3.5	—	—
[20]	1	2–6 GHz	68 × 44	< −20 dB	4.8		—
	2	2.3–6.0 GHz	76 × 76	< −20 dB	5	0.01	—
	4	2.0–6.0 GHz	124 × 124	< −30 dB	3.1–6.75	0.03	—
[21]	4	3.4–3.6 GHz	150 × 75	< −15 dB	4.7 5	< 0.001	—
		4.8–5 GHz		< −15 dB			
[22]	4	3–6 GHz	150 × 74	< −15 dB	3.4–5.4	0.05	—
[23]	4	3.6–3.8 GHz	127 × 70	< −15 dB	1	0.01	—
Proposed	1	**3.26–3.39 GHz**	**55.56 × 52.92**	**-12 dB**	3.039	—	—
		5.47–5.75 GHz		**-24.54 dB**	3.219		
	2	**3.26–3.39 GHz**	**55.56 × 105.84**	**-14.4 dB**	3.196	< 0.014	9.99
		5.47–5.75 GHz		**-24.94 dB**	3.213		9.99
	4	**3.26–3.39 GHz**	**111.12 × 105.84**	**-16.3 dB**	3.161	< 0.003	9.99
		5.47–5.75 GHz		**-26.82 dB**	3.161		9.99
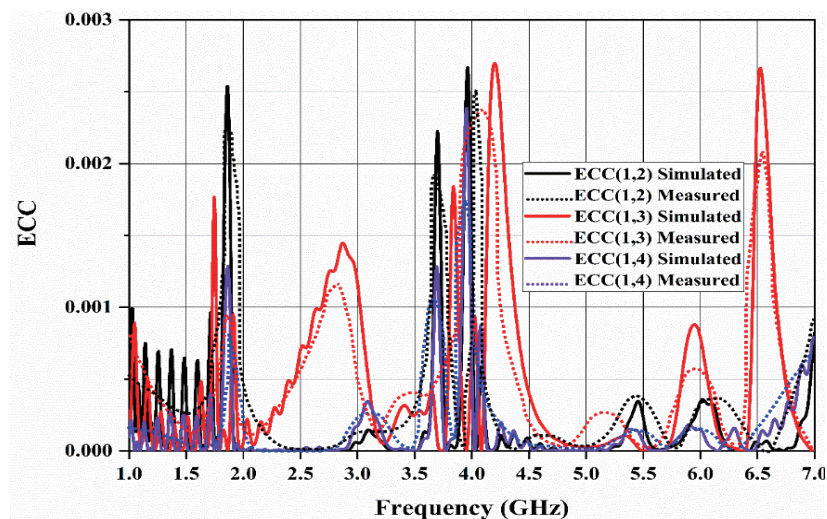
FIGURE 28. ECC of a quad-port serrated microstrip MIMO antenna.

Figure 28 denotes the ECC of the four-element serrated microstrip patch antenna. From Figure 27, the DG value of the dual-port serrated microstrip MIMO antenna is observed to be 9.90 which meets the MIMO diversity criteria. In addition, the measured antenna's ECCs are less than 0.001 at both the resonant frequency bands.

Table 3 compares the serrated microstrip MIMO antenna to various MIMO antennas at sub-6 GHz in terms of its dimensions, S_{11}, gain, ECC, and DG. The antenna in [21] covers dual bands with more gain, but the MIMO antenna is not manufactured. The antenna in [17] covers 4 bands, but the antenna occupies more space, and it does not cover the sub-6 GHz. MIMO antennas are proposed in [15–23], but they all have bigger size and offer less gain. The MIMO antenna shown in [20] with low S_{11} and low gain is compared with single element, 2×2 and 4×4 MIMO antennas. Chemical etching microstrip devices increase manufacturing efficiency and provide reduced fabrication costs. Thus, it can be seen that the proposed MIMO antennas with one, two, and four elements provide superior performance with respect to S_{11}, VSWR, 3D gain, and additional MIMO diversity characteristics such as DG and ECC.

4. CONCLUSION

Single port, dual-port, and quad-port serrated microstrip MIMO antennas were simulated and fabricated. S-parameters and MIMO diversity parameters were measured. This proposed single antenna functions at 3.30 GHz and 5.60 GHz with S_{11} of -12 dB and -24.54 dB. Two-port MIMO antenna resonates at 3.3 GHz and 5.6 GHz with S_{11} of -14.4 dB and -24.94 dB, and four-port MIMO antenna resonates at 3.3 GHz and 5.6 GHz with S_{11} of -16.3 dB and -26.82 dB. For a dual-port MIMO antenna, the isolation is -28.04 dB at 3.30 GHz and -26.53 dB at 5.60 GHz. For a quad-port MIMO antenna, the isolation is -42.53 dB at 3.30 GHz and -34 dB at 5.6 GHz. Along with S-parameters, MIMO diversity parameters were also measured. ECC is less than 0.0025 and 0.001 at the two resonant frequency bands and for the two MIMO antennas. DG is 9.93 dB for two-element and 9.90 dB for four-element MIMO antenna. These parameters make the antenna fit for intelligent devices utilizing sub-6 GHz 5G in IOT applications.

REFERENCES

[1] Kumar, S., A. S. Dixit, R. R. Malekar, H. D. Raut, and L. K. Shevada, "Fifth generation antennas: A comprehensive review of design and performance enhancement techniques," *IEEE Access*, Vol. 8, 163 568–163 593, 2020.

[2] Tütüncü, B. and M. Kösem, "Substrate analysis on the design of wide-band antenna for sub-6 GHz 5G communication," *Wireless Personal Communications*, Vol. 125, No. 2, 1523–1535, 2022.

[3] Kiruthika, R. and T. Shanmuganantham, "Comparison of different shapes in microstrip patch antenna for X-band applications," in *2016 International Conference on Emerging Technological Trends (ICETT)*, 1–6, Kollam, India, 2016.

[4] Abdul-Rahman, E. and D. N. Aloi, "Design of a 5G sub-6 GHz vehicular cellular antenna element with consistent radiation pattern using characteristic mode analysis," *Sensors*, Vol. 22, No. 22, 8862, 2022.

[5] Keriee, H., M. K. A. Rahim, O. Ayop, N. A. Nayyef, M. Ghanim, O. R. Alobaidi, B. Esmail, and Y. M. Hussein, "A slotted planar antenna for 5G applications," *ELEKTRIKA — Journal of Electrical Engineering*, Vol. 21, No. 2, 11–14, 2022.

[6] Karthikeyan, M., R. Sitharthan, T. Ali, S. Pathan, J. Anguera, and D. S. Sundar, "Stacked T-shaped strips compact antenna for WLAN and WiMAX applications," *Wireless Personal Communications*, Vol. 123, 1523–1536, 2022.

[7] Sharawi, M. S., A. B. Numan, and D. N. Aloi, "Isolation improvement in a dual-band dual-element MIMO antenna system using capacitively loaded loops," *Progress In Electromagnetics Research*, Vol. 134, 247–266, 2013.

[8] Dkiouak, A., A. Zakriti, and M. E. Ouahabi, "Design of a compact dual-band MIMO antenna with high isolation for WLAN and X-band satellite by using orthogonal polarization," *Journal of Electromagnetic Waves and Applications*, Vol. 34, No. 9, 1254–1267, 2020.

[9] Deng, J., J. Li, L. Zhao, and L. Guo, "A dual-band inverted-F MIMO antenna with enhanced isolation for WLAN applications," *IEEE Antennas and Wireless Propagation Letters*, Vol. 16, 2270–2273, 2017.

[10] Shoaib, S., I. Shoaib, N. Shoaib, X. Chen, and C. G. Parini, "Design and performance study of a dual-element multiband printed monopole antenna array for MIMO terminals," *IEEE Antennas and Wireless Propagation Letters*, Vol. 13, 329–332, 2014.

[11] Yang, Y., Q. Chu, and C. Mao, "Multiband MIMO antenna for GSM, DCS, and LTE indoor applications," *IEEE Antennas and Wireless Propagation Letters*, Vol. 15, 1573–1576, 2016.

[12] Moradikordalivand, A., C. Y. Leow, T. A. Rahman, S. Ebrahimi, and T. H. Chua, "Wideband MIMO antenna system with dual polarization for WiFi and LTE applications," *International Journal of Microwave and Wireless Technologies*, Vol. 8, No. 3, 643–650, 2016.

[13] Chattha, H. T., "4-port 2-element MIMO antenna for 5G portable applications," *IEEE Access*, Vol. 7, 96 516–96 520, 2019.

[14] Desai, A., M. Palandoken, I. Elfergani, I. Akdag, C. Zebiri, J. Bastos, J. Rodriguez, and R. A. Abd-Alhameed, "Transparent 2-element 5G MIMO antenna for sub-6 GHz applications," *Electronics*, Vol. 11, No. 2, 251, 2022.

[15] Srivastava, K., A. Kumar, B. K. Kanaujia, S. Dwari, and S. Kumar, "A CPW-fed UWB MIMO antenna with integrated GSM band and dual band notches," *International Journal of RF and Microwave Computer-Aided Engineering*, Vol. 29, No. 1, e21433, 2019.

[16] Sarkar, D. and K. V. Srivastava, "Four element dual-band sub-6 GHz 5G MIMO antenna using SRR-loaded slot-loops," in *2018 5th IEEE Uttar Pradesh Section International Conference on Electrical, Electronics and Computer Engineering (UPCON)*, 1–5, Gorakhpur, India, 2018.

[17] Jha, K. R., Z. A. P. Jibran, C. Singh, and S. K. Sharma, "4-port MIMO antenna using common radiator on a flexible substrate for sub-1 GHz, sub-6 GHz 5G NR, and Wi-Fi 6 applications," *IEEE Open Journal of Antennas and Propagation*, Vol. 2, 689–701, 2021.

[18] Thanuku, N., S. A. Kumar, and T. Shanmuganantham, "Design of 4-element MIMO antenna for ISM band applications," in *2019 IEEE Indian Conference on Antennas and Propogation (InCAP)*, 1–4, Ahmedabad, India, 2019.

[19] Parchin, N. O., Y. I. A. Al-Yasir, A. M. Abdulkhaleq, H. J. Basherlou, A. Ullah, and R. A. Abd-Alhameed, "A New broadband MIMO antenna system for sub 6 GHz 5G cellular Communications," in *2020 14th European Conference on Antennas and Propagation (EuCAP)*, 1–4, Copenhagen, Denmark, 2020.

[20] Chakraborty, S., M. A. Rahman, M. A. Hossain, A. T. Mobashsher, E. Nishiyama, and I. Toyoda, "A 4-element MIMO antenna with orthogonal circular polarization for sub-6 GHz 5G cellular applications," *SN Applied Sciences*, Vol. 2, 1–13, 2020.

[21] Govardhani, I., M. V. Narayana, A. Navya, A. Venkatesh, S. C. Spurjeon, S. S. Venkat, and S. Sanjay, "Design of high directional crossed dipole antenna with metallic sheets for UHF and VHF applications," *International Journal of Engineering & Technology*, Vol. 7, No. 1.5, 42–50, 2017.

[22] Imamdi, G., M. V. Narayan, A. Navya, and A. Roja, "Reflector array antenna design at millimetric (mm) band for on the move applications," *ARPN Journal of Engineering and Applied Sciences*, Vol. 13, No. 1, 352–359, 2018.

[23] Immadi, G., M. V. Narayana, A. Navya, C. A. Varma, A. A. Reddy, A. M. Deepika, and K. Kavya, "Analysis of substrate integrated frequency selective surface antenna for IoT applications," *Indonesian Journal of Electrical Engineering and Computer Science*, Vol. 18, No. 2, 875–881, 2020.

[24] Kumar, M. N., M. V. Narayana, G. Immadi, P. Satyanarayana, and A. Navya, "Analysis of a low-profile, dual band patch antenna for wireless applications," *AIMS Electronics and Electrical Engineering*, Vol. 7, No. 2, 171–186, 2023.

[25] Reddy, K. H., M. V. Narayana, G. Immadi, P. Satyanarayana, K. Rajkamal, and A. Navya, "A low-profile electrically small antenna with a circular slot for global positioning system applications," *Progress In Electromagnetics Research C*, Vol. 133, 27–38, 2023.

[26] Rao, L. N., G. Immadi, M. R. V. Narayana, A. Navya, A. S. Madhuri, and K. Rajkamal, "A compact multiband hybrid rectangular DRA for wireless applications," *Progress In Electromagnetics Research Letters*, Vol. 117, 89–96, 2024.

[27] Majji, N. K., V. N. Madhavareddy, G. Immadi, N. Ambati, and S. M. Aovuthu, "Analysis of a compact electrically small antenna with SRR for RFID applications," *Engineering, Technology & Applied Science Research*, Vol. 14, No. 1, 12 457–12 463, Feb. 2024.

[28] Majji, N. K., V. N. Madhavareddy, G. Immadi, and N. Ambati, "A low-profile electrically small serrated rectangular patch antenna for rfid applications," *Engineering, Technology & Applied Science Research*, Vol. 14, No. 2, 13 611–13 616, Apr. 2024.